agriculture

MDPI

Article

Monitoring *Sitobion avenae* Infestations in Winter Wheat Using UAV-Obtained RGB Images and Deep Learning

Atanas Z. Atanasov [1], Boris I. Evstatiev [2,*], Asparuh I. Atanasov [3], Plamena D. Nikolova [1] and Antonio Comparetti [4]

[1] Department of Agricultural Machinery, Agrarian and Industrial Faculty, University of Ruse "Angel Kanchev", 7017 Ruse, Bulgaria; aatanasov@uni-ruse.bg (A.Z.A.); pdnikolova@uni-ruse.bg (P.D.N.)
[2] Department of Automatics and Electronics, Faculty of Electrical Engineering, Electronics, and Automation, University of Ruse "Angel Kanchev", 7017 Ruse, Bulgaria
[3] Department of Mechanics and Elements of Machines, Technical University of Varna, 9010 Varna, Bulgaria; asparuh.atanasov@tu-varna.bg
[4] Department of Agricultural, Food and Forest Sciences, University of Palermo, Viale delle Scienze, Building 4, Office n. 137, 90128 Palermo, Italy; antonio.comparetti@unipa.it
* Correspondence: bevstatiev@uni-ruse.bg

Abstract

The grain aphid (*Sitobion avenae*) is a major pest of winter wheat, causing significant yield losses through direct feeding and as a vector of barley yellow dwarf virus (BYDV). Populations can increase rapidly under moderate temperatures and low rainfall, potentially leading to severe infestations if not effectively monitored and managed. This study develops and validates a UAV-based RGB imaging methodology, which relies on deep learning for accurate detection and assessment of *Sitobion avenae* in wheat crops. The RGB images are preliminarily filtered using "histogram equalization", which allows for highlighting the infested areas. An experimental study was conducted under the specific climatic conditions of Southern Dobruja, Bulgaria, to quantify *Sitobion avenae* infestations. Three neural network architectures were used (DeepLabv3, U-Net, and PSPNet) in combination with three backbone models: ResNet34, ResNet50, and ResNet101. The optimal combination was determined to be the U-Net + ResNet101 model, which achieved an average F1 score of 0.982 and a Cohen's Kappa coefficient of 0.966. The results demonstrate that UAV-based detection allows precise mapping of infested areas, enabling targeted insecticide applications and effective pest management while substantially reducing chemical inputs. These findings indicate that the proposed framework provides a reliable and scalable tool for precision pest monitoring and control in winter wheat.

Keywords: assessment; detection; classification; pest monitoring; precision agriculture

Academic Editor: Jiehao Li

Received: 5 February 2026
Revised: 25 February 2026
Accepted: 10 March 2026
Published: 11 March 2026

1. Introduction

Winter wheat (*Triticum aestivum*) is one of the most important cereal crops, occupying approximately 220 million hectares worldwide, and plays a key role in maintaining food and feed security in many countries [1,2]. In smaller countries such as Bulgaria, wheat accounts for about 32% of the total cultivated crop area [3]. Ensuring optimal conditions for its cultivation is therefore essential for achieving high yields.

Global climate change and increasing climatic instability in recent years [4–7] have created favorable conditions for the rapid and widespread occurrence of numerous diseases and pests in wheat crops across many regions. Among the most common wheat pests

directly influenced by climate change are wheat aphids, including *Rhopalosiphum padi*, *Schizaphis graminum*, *R. maidis*, *Metopolophium dirhodum*, *Sitobion avenae*, and *Diuraphis noxia*. Two of these species, commonly known as the Russian wheat aphid (*Diuraphis noxia*) and the bird cherry–oat aphid (*Rhopalosiphum padi*), are particularly notorious due to the significant direct and indirect damage they cause to wheat [8].

The timely detection of aphid infestations and the implementation of appropriate plant protection measures are crucial for effective pest control. Traditional invasive detection methods [9,10] are sufficiently accurate and reliable; however, they are labor-intensive, subjective, and time-consuming, often requiring specialized laboratory facilities and well-trained personnel. These limitations may lead to delays in the decision-making process for plant protection interventions.

In recent years, advances in smart technologies have substantially reduced the constraints associated with labor-intensive and invasive methods for detecting crop diseases and pests [11]. Considerable research has been conducted on monitoring wheat diseases, such as yellow rust, using unmanned aerial vehicles (UAVs) and deep learning techniques [12–18]. In contrast, studies focusing on insect infestations, particularly wheat aphids, remain relatively limited.

Nevertheless, several studies [19–23] have demonstrated the effectiveness of UAVs for monitoring insect infestations in various crops. UAV platforms enable rapid acquisition of spatial data through imagery, which can subsequently be analyzed using artificial intelligence (AI) algorithms. UAV-based monitoring offers multiple advantages, including large-area coverage, reduced labor requirements, and high temporal and spatial resolution. However, the effectiveness of such systems is influenced by factors such as the cost, resolution, and spectral sensitivity of onboard sensors, as well as environmental conditions during data acquisition.

High-resolution hyperspectral imaging has emerged as a reliable method for detecting insect infestations. For example, studies using a pistol-grip fiber holder attached to a portable spectroradiometer have successfully applied hyperspectral remote sensing combined with machine learning (ML) techniques to differentiate between healthy and aphid-infested wheat canopies [24]. Despite the high potential of this approach for early detection and classification of aphid infestations in winter wheat, its practical application over large agricultural areas remains challenging due to logistical and operational constraints. Additional research has further confirmed the strong potential of hyperspectral imaging for species-level classification [25]. A study assessing the severity of damage caused by the cereal leaf beetle (*Oulema melanopus* L., Coleoptera: Chrysomelidae) using hyperspectral remote sensing and machine learning was presented by [26].

Although hyperspectral imaging provides exceptional accuracy for detecting and monitoring insect pests, to date, no published studies have demonstrated its direct application using UAV platforms for field-scale monitoring of aphid infestations or other small insects. Furthermore, the high cost of hyperspectral sensors and the need for specialized training represent significant barriers to their widespread practical use.

To overcome the limitations associated with hyperspectral cameras, several studies propose alternative, more affordable approaches based on multispectral imaging. Panopoulou et al. [27], for instance, investigated the detection of *Xylotrechus chinensis* infestation in mulberry trees using UAV-acquired multispectral images analyzed through machine learning and vegetation indices (NDVI, NDRE, EVI) to classify healthy and infested trees. Similar applications of UAV platforms equipped with multispectral sensors for analyzing vegetation indices and monitoring crop health, growth, and insect-induced stress are discussed by [28]. Other researchers [29] propose an integrated approach for mapping insect pest infestations in crops using UAVs, multispectral imagery, and deep learning techniques.

A promising alternative approach for the early detection of aphid infestations using a low-cost electronic nose (E-nose), near-infrared spectroscopy, and machine learning modeling has been proposed by [30].

Despite the considerable progress in applying remote sensing and machine learning techniques for crop health monitoring, important research gaps remain in the detection of aphid infestations in winter wheat. Most existing studies focus on plant diseases or assess insect-induced stress indirectly through vegetation indices derived from multispectral or hyperspectral data. In contrast, the direct detection and assessment of aphid infestations using UAV-acquired RGB imagery and deep learning under real field conditions have received limited attention.

Furthermore, many studies rely on high-cost hyperspectral sensors or controlled experimental settings, which restricts the scalability and practical applicability of these approaches. Low-cost, operational solutions suitable for routine agricultural monitoring are still insufficiently explored, particularly in regions with distinct agro-climatic conditions.

Southern Dobruja, Bulgaria, is characterized by a continental climate with increasing variability in temperature and precipitation, frequent droughts, and prolonged heat stress during the growing season. These conditions favor the rapid development of aphid populations in winter wheat, yet region-specific studies employing UAV-based imaging and artificial intelligence for aphid monitoring are lacking.

Therefore, there is a clear need for robust, cost-effective, and regionally adapted methodologies capable of detecting and assessing aphid infestations under heterogeneous field conditions using readily available UAV platforms.

The main objective of this study is to develop and validate a methodology for the detection and assessment of grain aphid (*Sitobion avenae*) infestations in winter wheat using UAV-acquired RGB imagery and deep learning techniques.

2. Materials and Methods

2.1. Object and Means of the Study

The study was conducted during the 2024–2025 vegetation season in the Southern Dobrudzha region, located in northeastern Bulgaria, within the production areas of the agricultural cooperative Zlatno Zarno, situated near the village of Kalipetrovo (44°04′50.96″ N, 27°14′11.89″ E), at an average elevation of 82 m a.s.l. The regional climate is temperate continental, characterized by a mean annual air temperature of 10.2 °C and an average annual precipitation of approximately 571 mm, which is unevenly distributed throughout the year. According to ref. [31], the occurrence of pests in crops is strongly influenced by climate change. During the 2024–2025 season, the region's mild temperatures and moderately warm, moderately humid periods likely favored the development of the English grain aphid (*Sitobion avenae*), while localized rain events temporarily affected their distribution. The predominant soil types in the region are leached and carbonate chernozems, which are highly suitable for cereal crop production [32].

The cooperative cultivates crops typical for the region, including wheat, maize, sunflower, and rapeseed, with a total cultivated area of approximately 1800 ha. Two soil management systems are implemented in the cooperative's production practice: conventional tillage and subsoiling.

The experimental investigation was carried out on a field planted with the winter wheat variety Avenue (selection of the company Limagrain, Saint-Beauzire, France) (Figure 1), covering a total area of 44.6 ha and located within a 0.8 km radius of the cooperative's farmyard. Two soil cultivation technologies were applied before sowing: (1) conventional primary tillage using a disk harrow at a depth of 25 cm, performed with a Carrier disk harrow by Väderstad (Mjölby, Sweden) mounted on a Magnum 340 tractor

by Case IH (Racine, WI, USA), and (2) subsoiling at a depth of 27 cm, carried out using a Karat 9 deep cultivator by LEMKEN GmbH & Co. (Alpen, Germany), operated with the same tractor model.

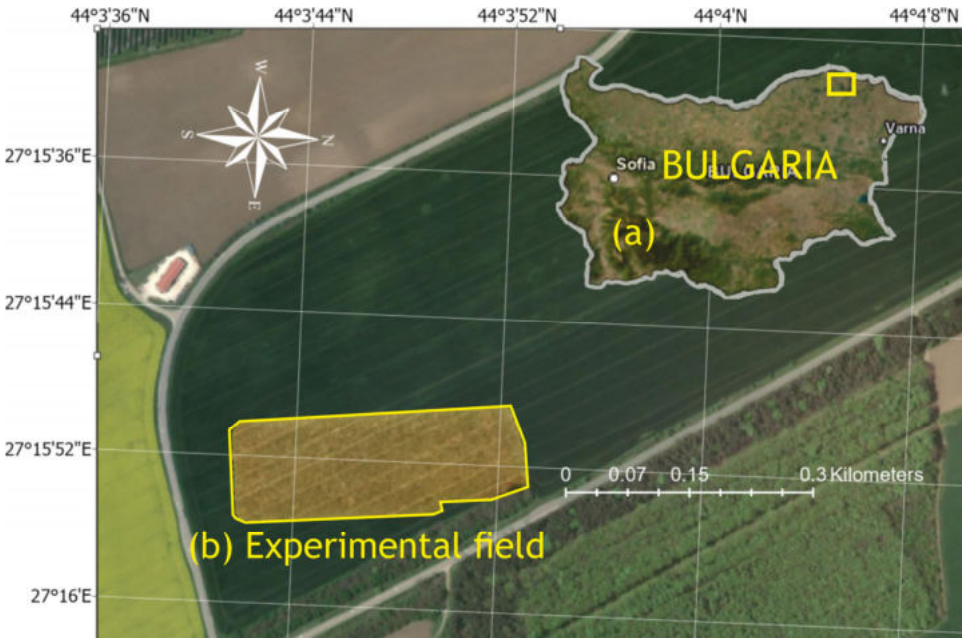

Figure 1. Geographic location and orientation of the experimental field.

Wheat sowing was conducted on 3 October 2024 at a seeding rate of 650 seeds m^{-2}, in accordance with the agrotechnical sowing window established for the region. The sowing operation was performed using a Väderstad Rapid 400S seed drill (Mjölby, Sweden), coupled with a Deutz-Fahr Agrotron 260 tractor (Lauingen, Bavaria, Germany).

2.2. UAV Flight Planning and Data Collection

A DJI Phantom 4 Multispectral unmanned aerial vehicle (Da-Jiang Innovations, Shenzhen, China), shown in Figure 2, was employed in this study. The platform is a quadcopter with vertical take-off and landing (VTOL) capability, enabling stable flight and precise positioning at low altitudes, which is essential for reliable multispectral data acquisition. Its operational configuration supports efficient flight mission planning and adequate spatial coverage within a single flight cycle.

The UAV is equipped with an integrated sensor system consisting of an RGB camera and a set of monochrome sensors fitted with narrow-band filters designed to capture key spectral regions in the visible and near-infrared domains. This sensor arrangement enables the acquisition of co-registered multispectral imagery suitable for subsequent photogrammetric and spectral analyses of surface and vegetation characteristics.

The camera system allows both nadir and oblique image acquisition, providing flexibility in mission design. The spatial resolution of the collected data, expressed as ground sample distance (GSD), is determined by the flight altitude, allowing adjustment according to the objectives of the survey. RGB and multispectral images are stored in standard file formats compatible with common processing workflows. Detailed technical specifications of the UAV platform and onboard sensors are summarized in Table 1 [33].

Figure 2. DJI Phantom 4 Multispectral unmanned aerial vehicle (UAV).

Table 1. Technical specifications of the UAV and onboard sensors.

Parameter	Specification
UAV model	DJI Phantom 4 Multispectral
Platform type	Quadcopter (VTOL)
Maximum flight time	~27 min
Sensor configuration	1 RGB + 5 multispectral
Sensor type	1/2.9″ CMOS
Image resolution	1600 × 1300 px
Spectral bands	B (450 ± 16 nm), G (560 ± 16 nm), R (650 ± 16 nm), RE (730 ± 16 nm), NIR (840 ± 26 nm)
Camera tilt range	−90° to +30°
Ground sample distance	H/18.9 cm·px^{-1}
Data format	JPEG (RGB), TIFF (MS)

Spatial information collection missions using the DJI Phantom 4 Multispectral UAV were conducted on 13 June 2025 within the cooperative's production fields, where an infestation of *Sitobion avenae* had been detected. The UAV flight on 13 June 2025 was conducted at the peak development stage of *Sitobion avenae*, providing a representative snapshot of infestation, although repeating flights at different growth stages could improve model robustness by capturing temporal dynamics. Flight planning was performed using the DJI Pilot software (version 2.5.1.17). The timing of the flights was coordinated with the preliminary weather forecast, which predicted suitable conditions for data collection between 12:00 and 14:30 local time. This is a common approach to minimize the impact of shading.

The UAV operated at a flight altitude of 80 m above ground level (AGL), maintaining a fixed heading angle of 90° relative to the terrain to ensure optimal coverage of the study area. To maximize the uniformity of image overlap and facilitate subsequent photogrammetric

processing, the flight trajectory was pre-planned with a front overlap of 80% and a side overlap of 70%. This configuration ensured proper alignment of images and high-quality multispectral data.

To monitor local weather conditions during the flights, a portable agrometeorological station Meteobot® (Meteobot, Varna, Bulgaria) was deployed in proximity to the study area. Meteorological parameters recorded during the mission included: wind speed 2.07 $m \cdot s^{-1}$, relative humidity 56.71%, air temperature 27 °C, solar radiation 751 $W \cdot m^{-2}$, and atmospheric pressure 1019.02 hPa, ensuring that UAV operations were conducted under stable environmental conditions.

Before the execution of the UAV flight missions, an extensive preliminary ground-truth survey of the 44.6-hectare study area was performed. This initial assessment, conducted by a specialist agronomist, confirmed that the localized infestation in wheat and observed physiological stress were specifically caused by the grain aphid (*Sitobion avenae*). Specifically, 25 ground-truth sampling points were established across the study area, covering both infested and non-infested zones, and all points were located within the UAV coverage area to ensure accurate correspondence between aerial and terrestrial observations. To document the spatial extent and morphology of the pest damage, high-resolution ground-level imagery was acquired using a G21 smartphone by Nokia (Espoo, Finland), leveraging its 50-megapixel main rear camera. These terrestrial photographs (Figure 3) provided a granular visual record of the infestation symptoms at the leaf and ear levels. This ground-truth dataset served as a vital reference for the subsequent calibration and validation of the multispectral UAV data, ensuring that the spectral anomalies detected by the aerial sensors were accurately correlated with the physical presence of *Sitobion avenae*.

Figure 3. A closer look at the grain aphid (*Sitobion avenae*).

To optimize the UAV battery usage and ensure focused data collection, a sub-area of the field with the highest severity of *Sitobion avenae* infestation was selected for aerial imaging. This section represented the most critical phytopathological condition within the total 44.6-hectare field, providing a representative dataset for subsequent analysis of pest distribution and severity.

2.3. Methodology of the Study

The study's methodology is summarized in Figure 4 and comprises six steps.

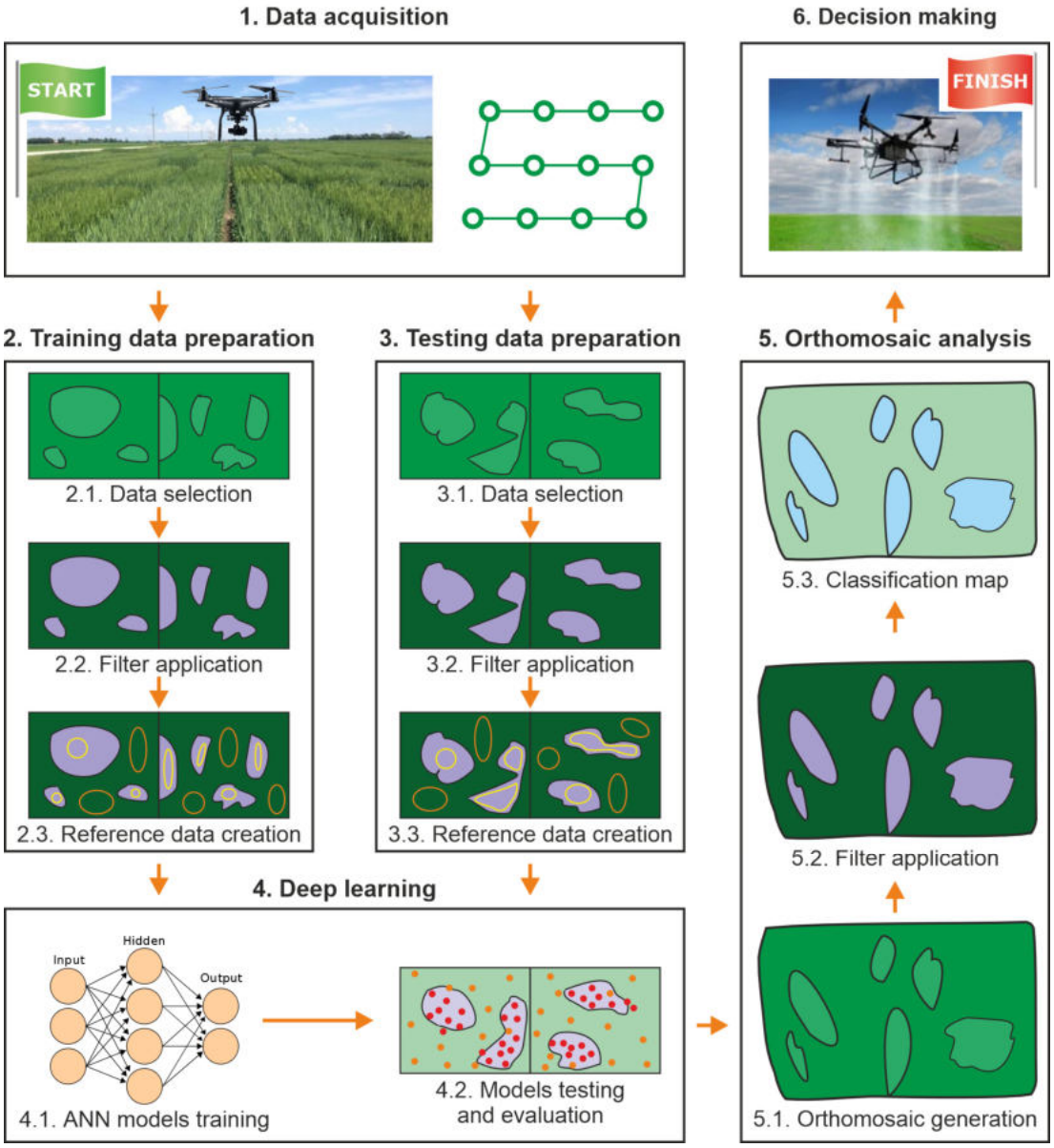

Figure 4. Summary of the study methodology.

Step 1. Data acquisition

The study begins by acquiring UAV-derived RGB data. The images made should have enough overlap in order to be able to create a qualitative orthomosaic from them. Lower height of the UAV flight is expected to improve the performance of the disease detection; however, it will reduce the scale of the investigated field. Therefore, an appropriate balance should be maintained between flight height, size of the field, and resolution of the camera used. In the current study, we have also collected other spectrum data in order to be able to generate an NDVI map; however, this is only for the purpose of initial comparison and assessment of the analyzed data.

Step 2. Training data preparation

This step is aimed at preparing data for training one or more neural-network-based models. It can be divided into three substeps:

(1) Data selection—Several images from those obtained in Step 1 are selected for the training (in this study, we have used four images). It is recommended that they are from different parts of the investigated field and do not have any overlapping areas. Furthermore, these images should adequately represent all typical situations that can be observed in the

field (healthy, infected, tractor tracks, artificial objects, etc.), i.e., when choosing the training images, it is important to try to keep the cumulative balance between classes as equal as possible. Thereafter, the selected images are merged together into one big image for further processing.

(2) Filter application—Next, the "histogram equalization" filter is applied to the merged training image. This can be done using different tools, but in this study, we are using Corel Photo-Paint's "Equalize" tool (Corel version v. 24.0.0.301). The reason for applying this filter is that a previous study [18] has shown that it allows for better highlighting of unhealthy regions in crop fields.

(3) Reference data creation—The final phase of this step is to create reference data on the training image with the filter applied. This is done by marking a region of interest (ROI) on the image of the following three classes:

- Healthy crop—no infestation is observed in this area.
- Infested crop—obvious *Sitobion avenae* infestation can be observed in the area.
- Tractor tracks—area of the field which has been damaged by tractors passing over it.

The reason for adding the third class is that many tractor tracks can be noticed on the images, which might impact the decision-making process.

Step 3. Testing data preparation

The third step is identical to the second one; however, different images are chosen from the initial dataset for validation purposes. It is recommended that these images should be from different parts of the field, i.e., they do not overlap with the training ones.

Similarly to Step 2, the chosen images are combined into a big one, the "histogram equalization" filter is applied, and ROI of the three classes are marked on it.

Step 4. Deep learning

In this step, different neural-network-based models are trained using the training data from Step 2. In the current study, we have chosen the following pixel-based models, supported in ArcGIS Pro v. 3.5.0 (Esri Inc., Redlands, CA, USA):

- U-Net—a neural network architecture used for image segmentation, which has shown good capabilities in crop identification [34], yellow rust detection [35], etc.
- DeepLab v3—a convolutional neural network for semantic segmentation, which has shown good capabilities in crop disease detection using RGB images [18].
- Pyramid Scene Parsing network (PSPNet)—a deep learning model, which has shown good capabilities for detecting diseases in wheat [36].

Furthermore, three backbones were used—ResNet34, ResNet50, and ResNet101.

A model is trained for each neural network + backbone combination, which is then tested on both the training and the testing data from Step 2 and Step 3, respectively. The performance of the model is evaluated using the following metrics:

- Precision—allows estimating the percentage of true positive pixels according to:

$$Precision = \frac{N_{TP}}{N_{TP} + N_{FP}}, \quad (1)$$

where N_{TP} and N_{FT} are the number of true positive and false positive pixels, respectively.

- Recall—allows estimating the percentage of correctly estimated pixels according to:

$$Recall = \frac{N_{TP}}{N_{TP} + N_{FN}}, \quad (2)$$

where N_{FN} is the number of false negative pixels.

- Cohen's Kappa—used for assessing the level of agreement between classified and reference pixels. It returns values between 0 (no agreement at all) and 1 (perfect agreement).

The values of the metrics are used to select the best-performing models, which are further compared using their confusion matrices to identify the optimal model.

Step 5. Orthomosaic analysis

The next stop is aimed at applying the optimal model to the orthomosaic. It includes three substeps:

(1) Orthomosaic generation—a high-definition orthomosaic is generated using the dataset obtained in Step 1.

(2) Filter application—the "histogram equalization" filter is applied on the generated orthomosaic, similarly to Steps 2 and 3.

(3) Classification map—the optimal models are applied on the filtered orthomosaic, and classification maps are generated. The classification maps are analyzed in detail to identify the best-performing model.

Step 6. Decision making

The final step in the methodology is to use the obtained classification map to identify the healthy and infested areas, their percentage, and the possible agro-technological routines applicable for the mitigation of the infestation. Such routines could include targeted insecticide application only in affected areas, thereby reducing chemical use and optimizing pest management.

3. Results and Discussion

3.1. Preliminary Analysis

An experimental study was conducted with the drone on 13 June 2025, as explained in the Methodology section. A total of 251 images were made in the visible and near-infrared spectrum, each (Step 1 of the methodology).

Next, according to Step 2, four images from the visible spectrum were selected and merged into a single image, as shown in Figure 5. On them can be observed darker areas, which represent the *Sitobion avenae* infestation, as well as tractor tracks. Next, the "histogram equalization" filter was applied to it, which allows for better highlighting of the infested areas, as can be seen from Figure 6a.

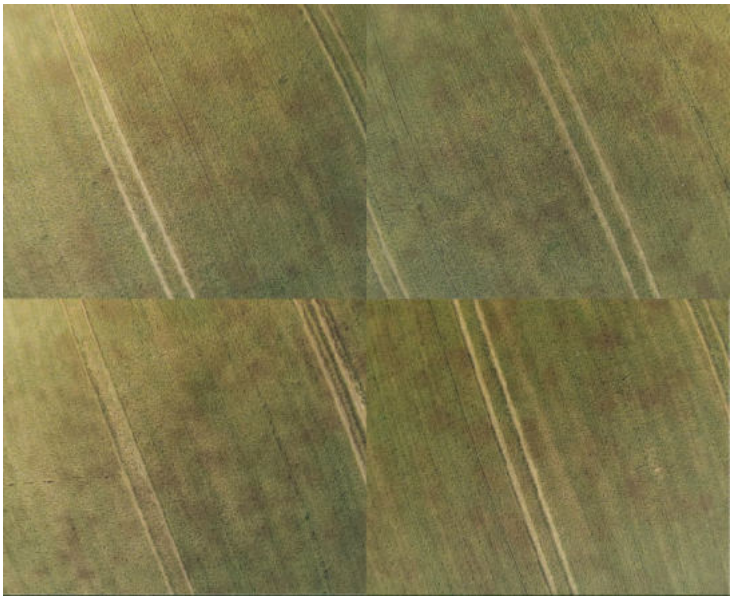

Figure 5. The chosen visual spectrum images, merged into a single image.

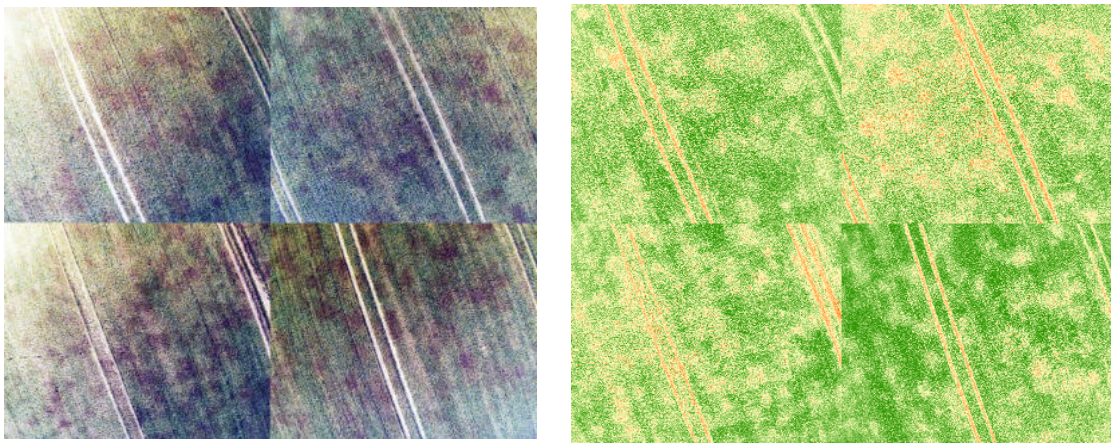

(**a**) (**b**)

Figure 6. The chosen training data represented as: (**a**) RGB map with histogram equalization filter applied; (**b**) NDVI map.

The obtained image is visually compared with an equivalent NDVI image (Figure 6b) that was constructed using the same areas in the red and near-infrared spectrum. This comparison allows the following observations to be made:

- Both approaches, based on NDVI and RGB with "histogram equalization", highlight unhealthy areas of the field. In the equalized RGB image, the unhealthy areas have a purplish color.
- The filtered RGB image allows a clear distinction between the infested area and tractor tracks, while the NDVI one does not, as they both appear with the same color scheme.

Next, reference data was prepared for the training image (Figure 7) by marking numerous points of interest (POI), corresponding to the three classes—healthy, infested, and tractor tracks. Only areas that can be clearly categorized in one of the three categories were marked as reference data, while areas whose class is uncertain were omitted.

Figure 7. Training images with an equalization filter applied and the training ROI marked: green—healthy crop; purple—infested crop; yellow—tractor tracks.

Similarly, four images were selected as testing data, merged into a single image, the "histogram equalization" filter was applied, and numerous POIs were marked on it in the three classes (Figure 8), according to Step 3 of the methodology.

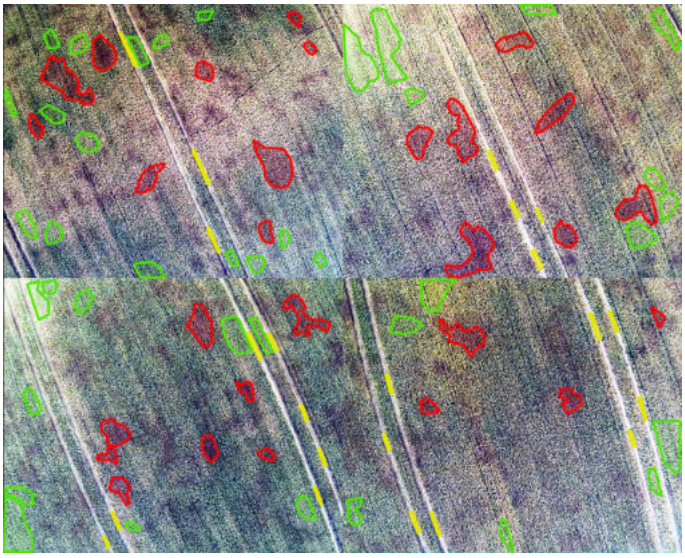

Figure 8. The testing images with equalization filter applied and the testing ROIs marked: green—healthy crop; red—infested crop; yellow—tractor tracks.

3.2. Model Training and Validation

Next, according to Step 4 of the methodology, a total of 9 models were trained using the three neural network architectures and 3 different backbones. It was implemented in the ArcGIS Pro software v. 3.5.0 developed by Esri Inc. (Redlands, CA, USA). The "Train Deep Learning Model" tool was used using "Set my own parameters". In the graphical user interface, the corresponding neural network and backbone models were chosen, and all other parameters were left to their default values.

The trained models were then applied to the training images for initial assessment of their performance. In Figure 9, the obtained classification maps are shown when using the trained U-Net models. It can be observed that the ResNet-50-based model performs slightly better in terms of identifying the tractor tracks, compared to the other two backbones. Furthermore, it can be visually observed that the identified infested area is larger with the ResNet-101-based model.

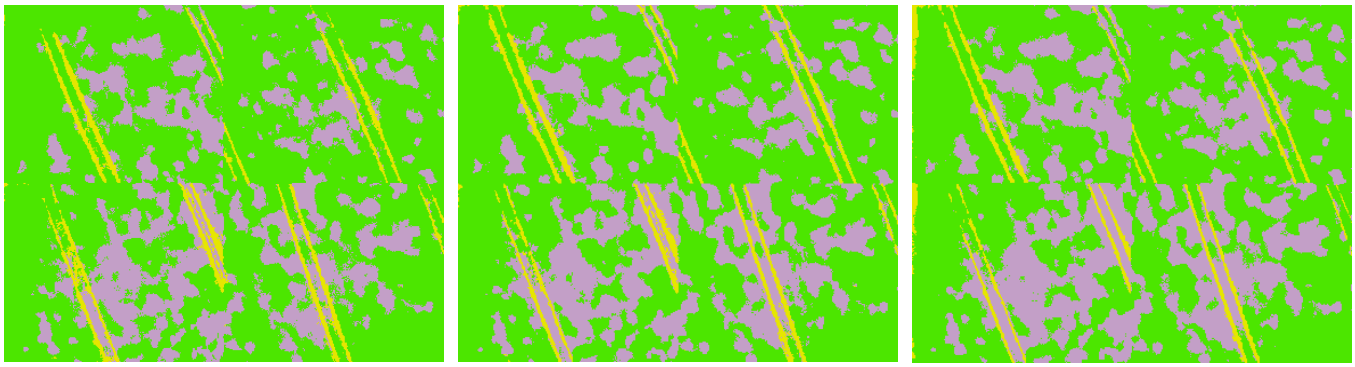

(**a**) (**b**) (**c**)

Figure 9. Results from the U-Net models training with backbones ResNet-34 (**a**), ResNet-50 (**b**), and ResNet-101 (**c**).

Figure 10 shows the classification maps of the training data when the DeepLab v3 architecture is used. It can be seen that the ResNet-34 and ResNet-50 maps are almost identical, while the ResNet-101-based model performs significantly worse with the tractor tracks identification.

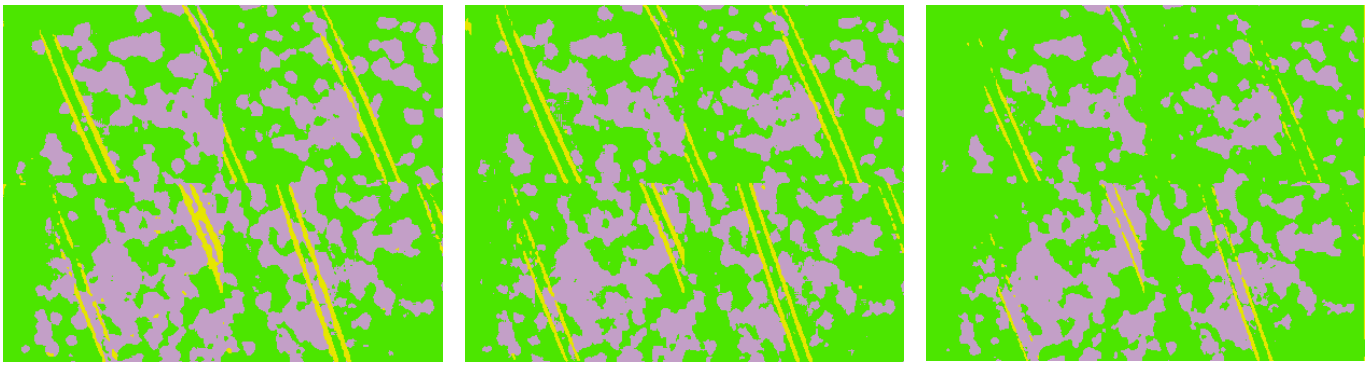

(**a**) (**b**) (**c**)

Figure 10. Results from the DeepLabv3 models training with backbones ResNet-34 (**a**), ResNet-50 (**b**), and ResNet-101 (**c**).

In Figure 11, the results from the application of the PSPNet models are shown. It can be visually observed that all models fail to properly identify the tractor tracks, and the ResNet-101-based one is a total disaster.

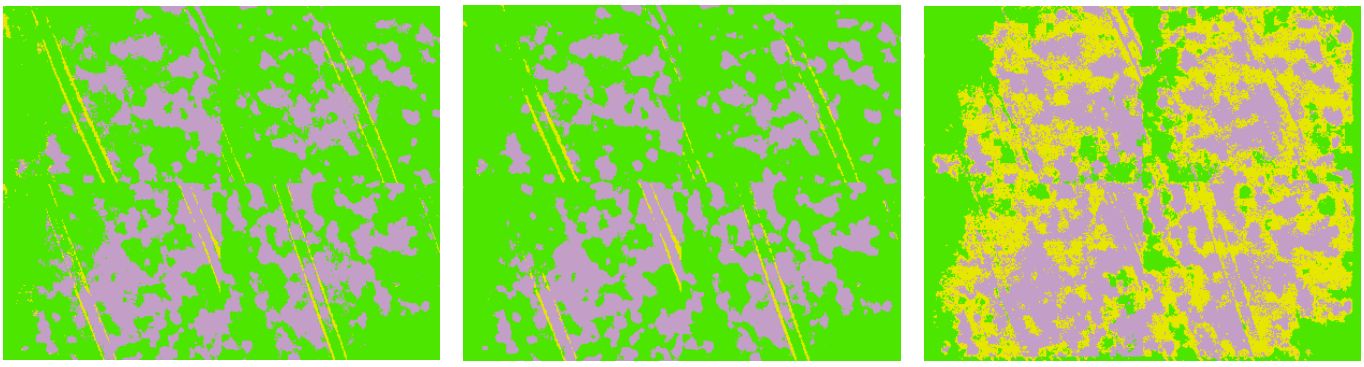

(**a**) (**b**) (**c**)

Figure 11. Results from the PSPNet models training with backbones ResNet-34 (**a**), ResNet-50 (**b**), and ResNet-101 (**c**).

The 9 models are compared in Table 2 using the adopted metric indicators. It can be seen that in terms of Average precision (average for the three classes) and Average recall, the best-performing models are DeepLabv3 + ResNet34, DeepLabv3 + ResNet50, and U-Net + ResNet50, with values of 0.997, 0.996, and 0.995, respectively. Similarly, the Cohen's Kappa measures are 0.994, 0.992, and 0.989, respectively. Furthermore, the table confirms that the PSPNet + ResNet101 model has the worst performance, with values of precision, recall, and Cohen's Kappa of 0.763, 0.797, and 0.648, respectively.

Table 2. Results from the assessment of the models' performance with the training data.

Model + Backbone	Average Precision	Average Recall	Cohen's Kappa
U-Net + ResNet34	0.991	0.991	0.981
U-Net + ResNet50	0.995	0.995	0.989
U-Net + ResNet101	0.980	0.980	0.958
DeepLabv3 + ResNet34	0.997	0.997	0.994
DeepLabv3 + ResNet50	0.996	0.996	0.992
DeepLabv3 + ResNet101	0.986	0.985	0.967
PSPNet + ResNet34	0.986	0.986	0.971
PSPNet + ResNet50	0.991	0.990	0.980
PSPNet + ResNet101	0.763	0.797	0.648

Next, to validate the models with independent data, the same procedure is repeated using the testing image. In Figure 12, the classification maps for the U-Net models are shown. The results are similar to those obtained with the training data with the ResNet-101-based model classifying larger areas as infested and performing worse when identifying tracks.

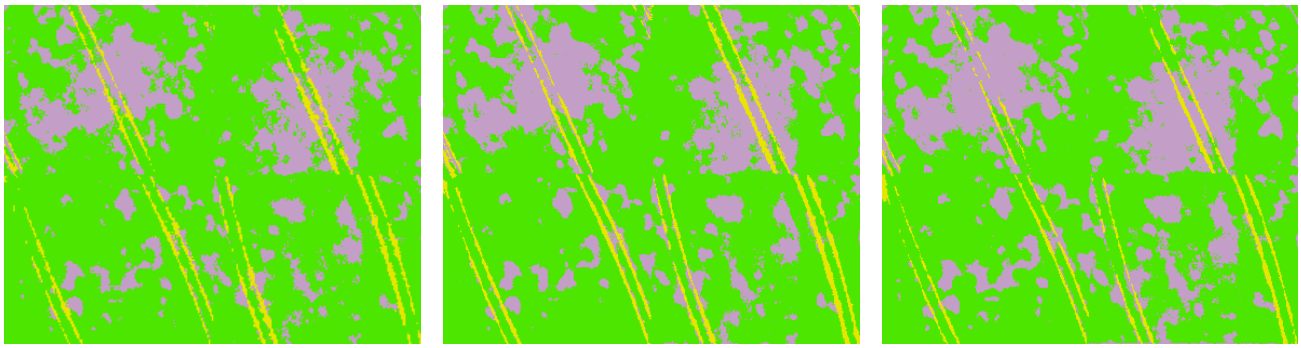

(**a**) (**b**) (**c**)

Figure 12. Results from the U-Net models testing with backbones ResNet-34 (**a**), ResNet-50 (**b**), and ResNet-101 (**c**).

In Figure 13, the classification results of the testing image can be observed, obtained with the DeepLab v3 models. Once again, it can be seen that the ResNet-50-based model has the best performance when identifying tractor tracs, while the ResNet-101 tracks identification is very low. Furthermore, the ResNet-34-based model has classified larger areas as infested, compared to the other two.

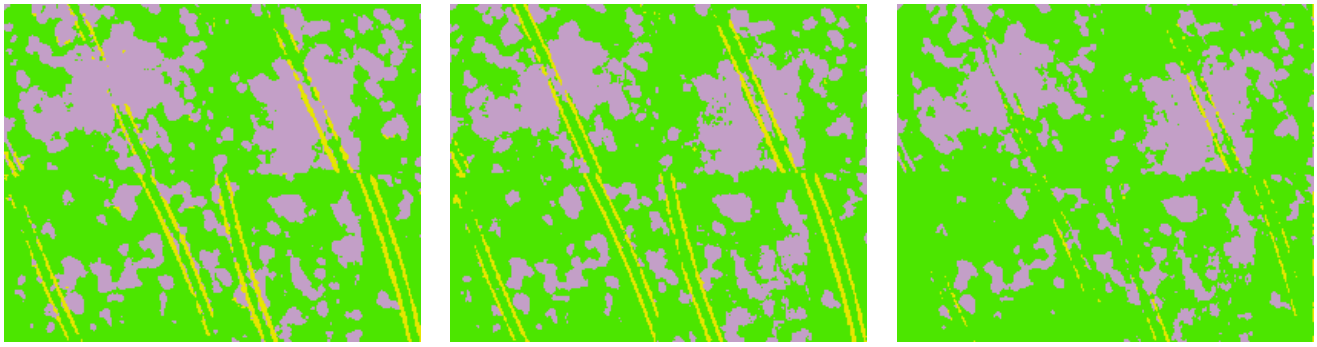

(**a**) (**b**) (**c**)

Figure 13. Results from the DeepLabv3 models testing with backbones ResNet-34 (**a**), ResNet-50 (**b**), and ResNet-101 (**c**).

Finally, the results from the PSPNet models are visualized in Figure 14. Once again, it is obvious that they fail to properly identify the tractor tracks, returning many false negatives, while the ResNet101-based model returned an enormous amount of true negatives.

The results from the performance of all models on the testing dataset are summarized in Table 3. This time, there are only two models with slightly higher performance than the others, the DeepLabv3 + ResNet50 and the DeepLabv3 + ResNet34-based ones. Their average precision, average recall, and Cohen's Kappa reach 0.993, 0.993, and 0.987, as well as 0.990, 0.990, and 0.982, respectively. Next, closely follows the U-Net + ResNet101 model with average precision, average recall, and Cohen's Kappa of 0.982, 0.982, and 0.966, respectively. The accuracy of the other models is lower, with the PSPNet-based models being the least accurate.

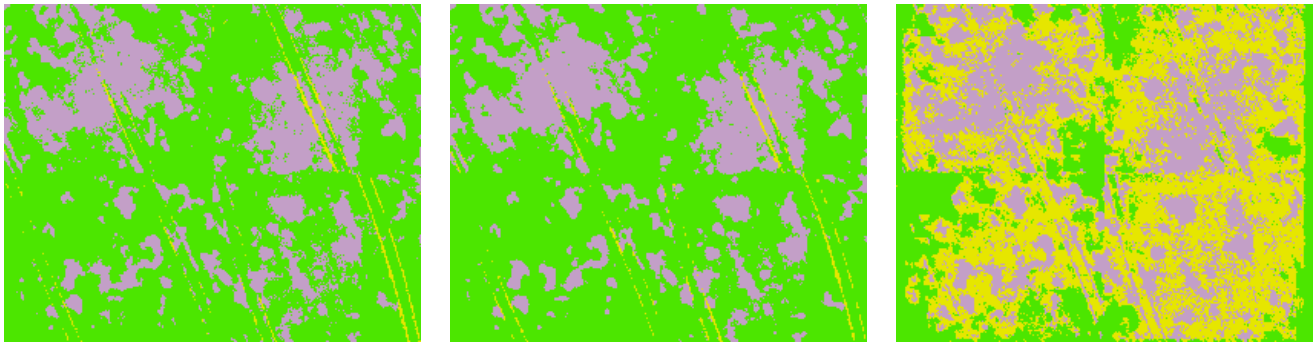

(**a**) (**b**) (**c**)

Figure 14. Results from the PSPNet models testing with backbones ResNet-34 (**a**), ResNet-50 (**b**), and ResNet-101 (**c**).

Table 3. Results from the performance assessment of the models with the testing data.

Model + Backbone	Average Precision	Average Recall	Cohen's Kappa
U-Net + ResNet34	0.971	0.970	0.944
U-Net + ResNet50	0.975	0.975	0.953
U-Net + ResNet101	**0.982**	**0.982**	**0.966**
DeepLabv3 + ResNet34	**0.990**	**0.990**	**0.982**
DeepLabv3 + ResNet50	**0.993**	**0.993**	**0.987**
DeepLabv3 + ResNet101	0.965	0.954	0.913
PSPNet + ResNet34	0.966	0.960	0.925
PSPNet + ResNet50	0.971	0.965	0.934
PSPNet + ResNet101	0.770	0.740	0.584

To get a deeper understanding of the differences between the three best-performing models, their confusion matrices are further evaluated and presented in Tables 4–6. It can be seen that the DeepLab models have approximately identical precisions for the infested and healthy classes, 0.988 and 0.997, respectively. The ResNet-50 slightly outperforms ResNet-34 in terms of recall of the infested class, but is slightly worse in the performance of the healthy class. The corresponding metrics of the U-Net model are lower by approximately 1/100.

Table 4. Confusion matrix of the DeepLabv3 model with ResNet-34 backbone.

		Predicted				Metrics		
		Infested	**Healthy**	**Tracks**	**∑**	**Precision**	**Recall**	**F1**
Actual	Infested	4545	14	17	4576	0.988	0.993	0.991
	Healthy	29	4979	8	5016	0.997	0.993	0.995
	Tracks	27	3	375	405	0.938	0.926	0.932
	Average values	4601	4996	400	9997	0.990	0.990	0.990

Table 5. Confusion matrix of the DeepLabv3 model with ResNet-50 backbone.

		Predicted				Metrics		
		Infested	**Healthy**	**Tracks**	**∑**	**Precision**	**Recall**	**F1**
Actual	Infested	4546	13	0	4559	0.988	0.997	0.993
	Healthy	55	4984	1	5040	0.997	0.989	0.993
	Tracks	0	1	402	403	0.998	0.998	0.998
	Average values	4601	4998	403	10,002	0.993	0.993	0.993

Table 6. Confusion matrix of the U-Net model with ResNet-101 backbone.

		Predicted				Metrics		
		Infested	**Healthy**	**Tracks**	**∑**	**Precision**	**Recall**	**F1**
Actual	Infested	4491	47	5	4543	0.976	0.989	0.982
	Healthy	109	4952	19	5080	0.991	0.975	0.983
	Tracks	0	0	379	379	0.940	1.000	0.969
	Average values	4600	4999	403	10,002	0.982	0.982	0.982

It can also be seen that the ResNet-50-based model outperforms the ResNet-34 one when it comes to the tractor tracks class, reaching values of 0.998/0.998 against 0.938/0.926. The precision and recall of the U-Net model with the tracks class are 0.940 and 1.000, respectively.

The validation of the three models shows that the DeepLabv3 + ResNet50 has the highest performance with the testing data, closely followed by DeepLabv3 + ResNet34 and U-Net + ResNet101.

3.3. Orthomosaic Analysis

Using the UAV-obtained RGB data, an orthomosaic was generated (Figure 15a) in ArcGIS Pro software v. 3.5.0 developed by Esri Inc. (Redlands, CA, USA). Thereafter, the orthomosaic was exported to a PNG image, and the "histogram equalization" filter was applied to it (Figure 15b) using Corel Photo-Paint v. 24.0.0.301, after which the modified image was imported back into ArcGIS Pro.

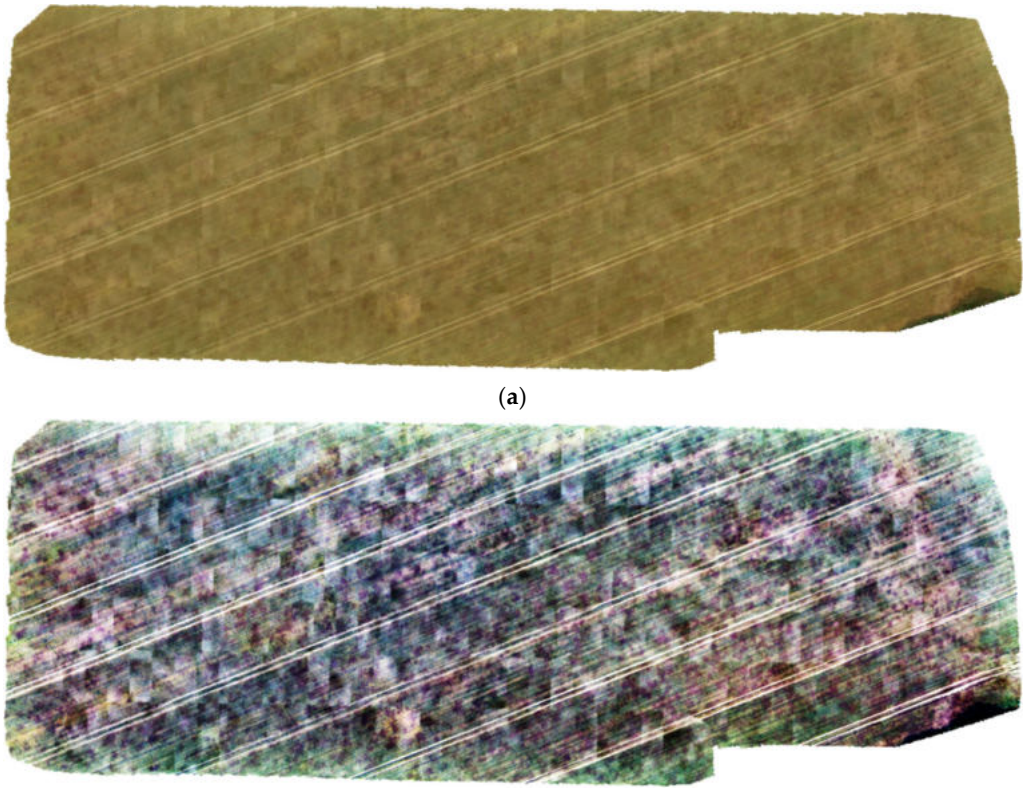

(**a**)

(**b**)

Figure 15. The generated orthomosaic before (**a**) and after (**b**) the "histogram equalization" filter is applied.

Next, the three best-performing models were applied to the equalized orthomosaic, and the corresponding classification maps were generated (Figure 16). It can be seen

that the two DeepLab models (Figure 16a,b) are returning an enormous number of false positives for the class "Tractor tracks". The reason for this is that there are many whitish spots on the equalized orthomosaic, which are very similar to the color of the tracks. In other words, even though the DeepLab models returned the highest accuracies during the training and validation process, they fail to properly analyze the actual orthomosaic.

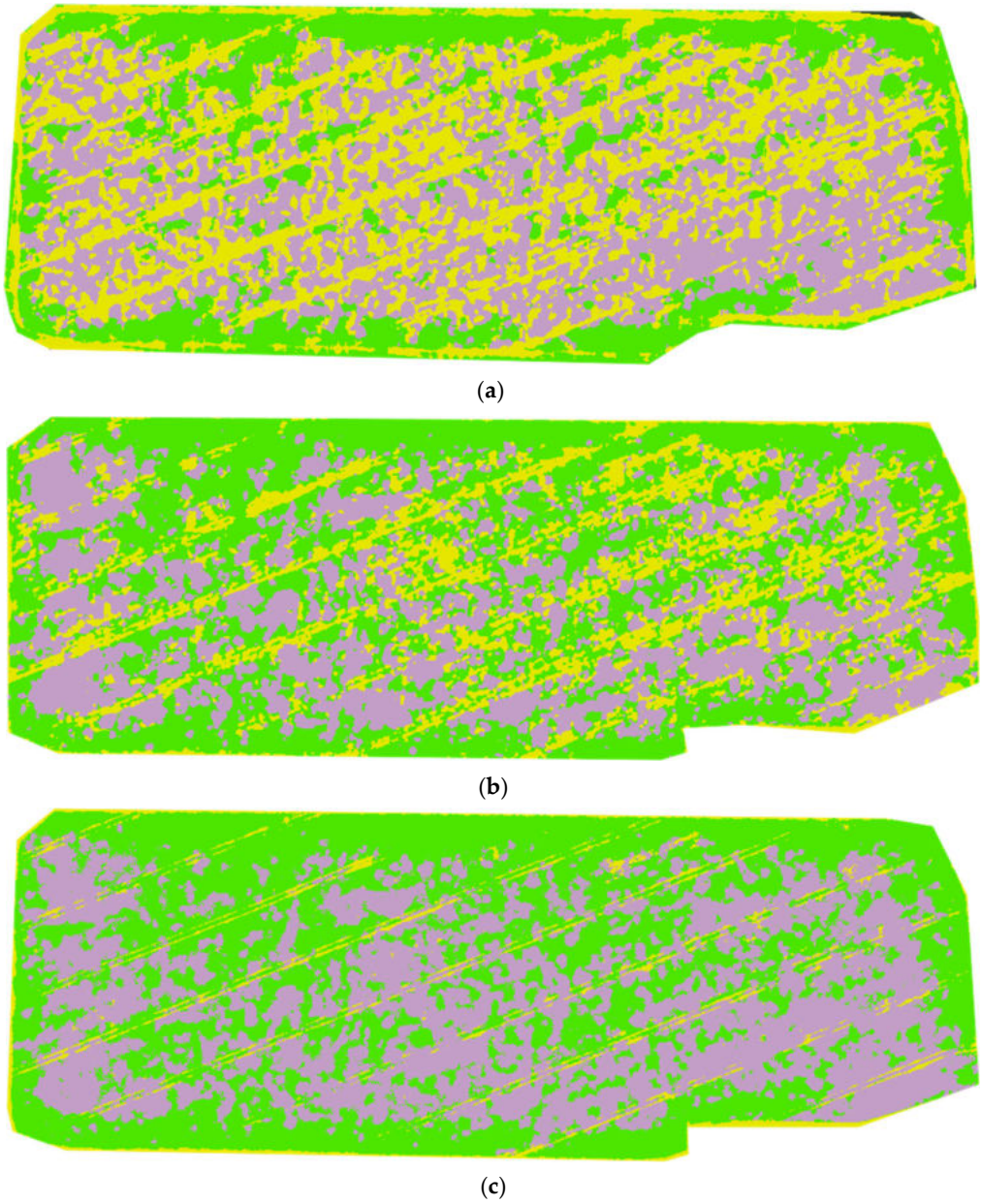

(**a**)

(**b**)

(**c**)

Figure 16. Classification maps created with: DeepLabv3 + ResNet34 (**a**); DeepLabv3 + ResNet50 (**b**); U-Net + ResNet101 (**c**). Legend: green—healthy; purple—infested; yellow—tractor tracks.

On the other hand, the classification map returned by the U-Net model with a ResNet101 backbone seems significantly better, as can be seen from Figure 16c. Even though the tractor tracks were not entirely identified, those that were identified closely represent the actual ones.

To get a better understanding of the problem, a strongly infested area of the orthomosaic has been zoomed in (Figure 17a), and the three classification maps were overlaid. As is already observable in Figure 6, the actual infested areas correspond to the purple spots, while all other areas are either not infested or represent tractor tracks. Figure 17b,c,

corresponding to DeepLab + ResNet34 and DeepLab + ResNet50 models, completely fails to properly classify the observed area. A large part of it is marked as tractor tracks, which is obviously not the case.

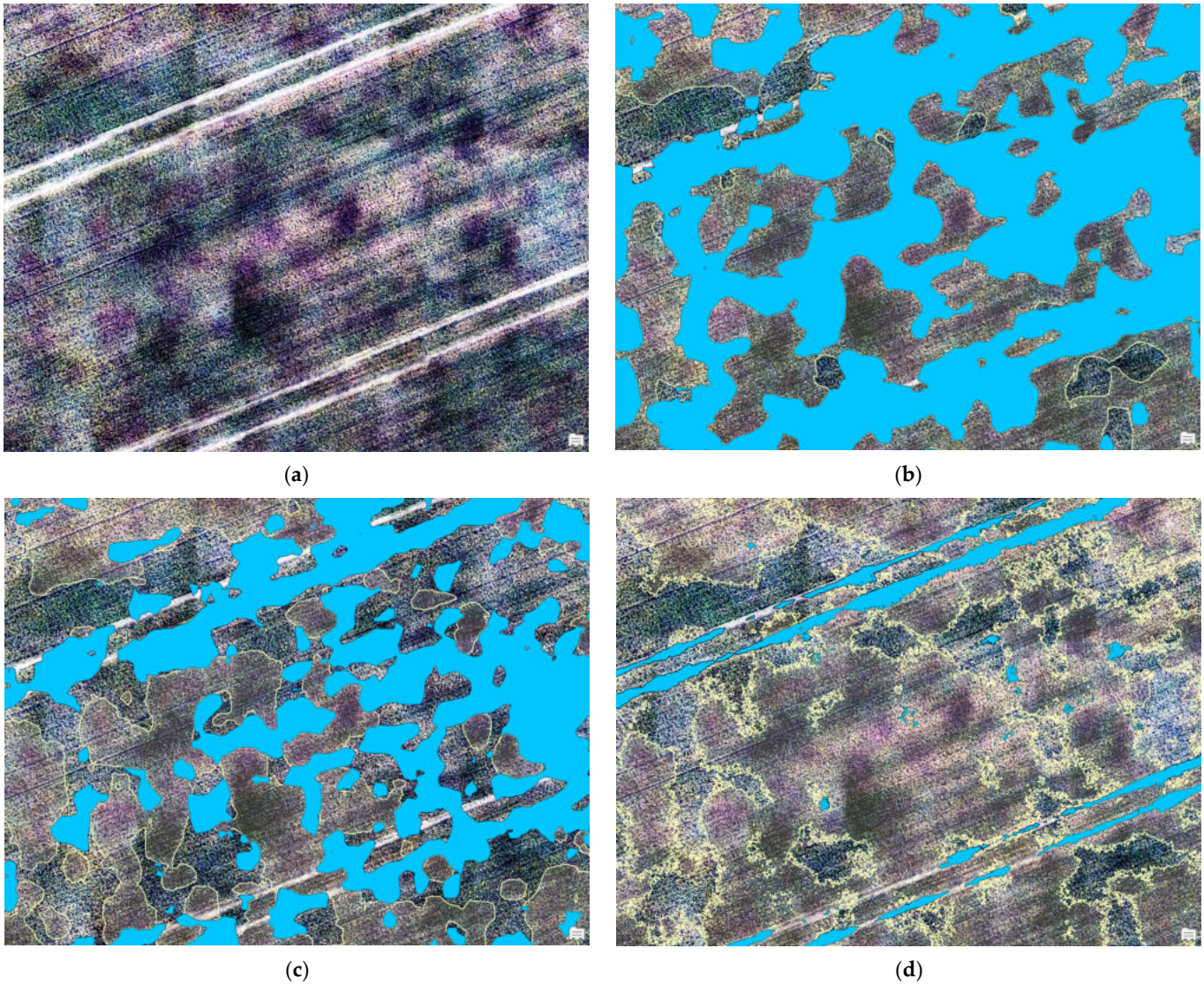

Figure 17. Close-up from the orthomosaic with an equalization filter applied (**a**) and the infested and (surrounded with yellow lines) and tracks (in blue) areas marked, respectively, by the DeepLabv3 + ResNet34 (**b**), DeepLabv3 + ResNet50 (**c**), and U-Net + ResNet101 (**d**) models.

On the other hand, the U-Net + ResNet101 model returns very good results (Figure 17d). Even though several false positives can be observed outside the actual tractor tracks, their area could be considered insignificant. Furthermore, it can be seen that the purplish areas are well-marked in yellow, i.e., the infested areas are properly identified.

However, another close-up of the orthomosaic, with a lower rate of infestation, is presented in Figure 18a. Once again, it can be seen that the two DeepLab models (Figure 18b,c) return an unacceptable rate of false positives in terms of tractor tracks. On the other hand, the U-Net-based model performs significantly better. Even though not all tracks were identified, there are almost no false positives. Furthermore, most of the infested (purplish) areas are properly identified, which is the main goal of the model.

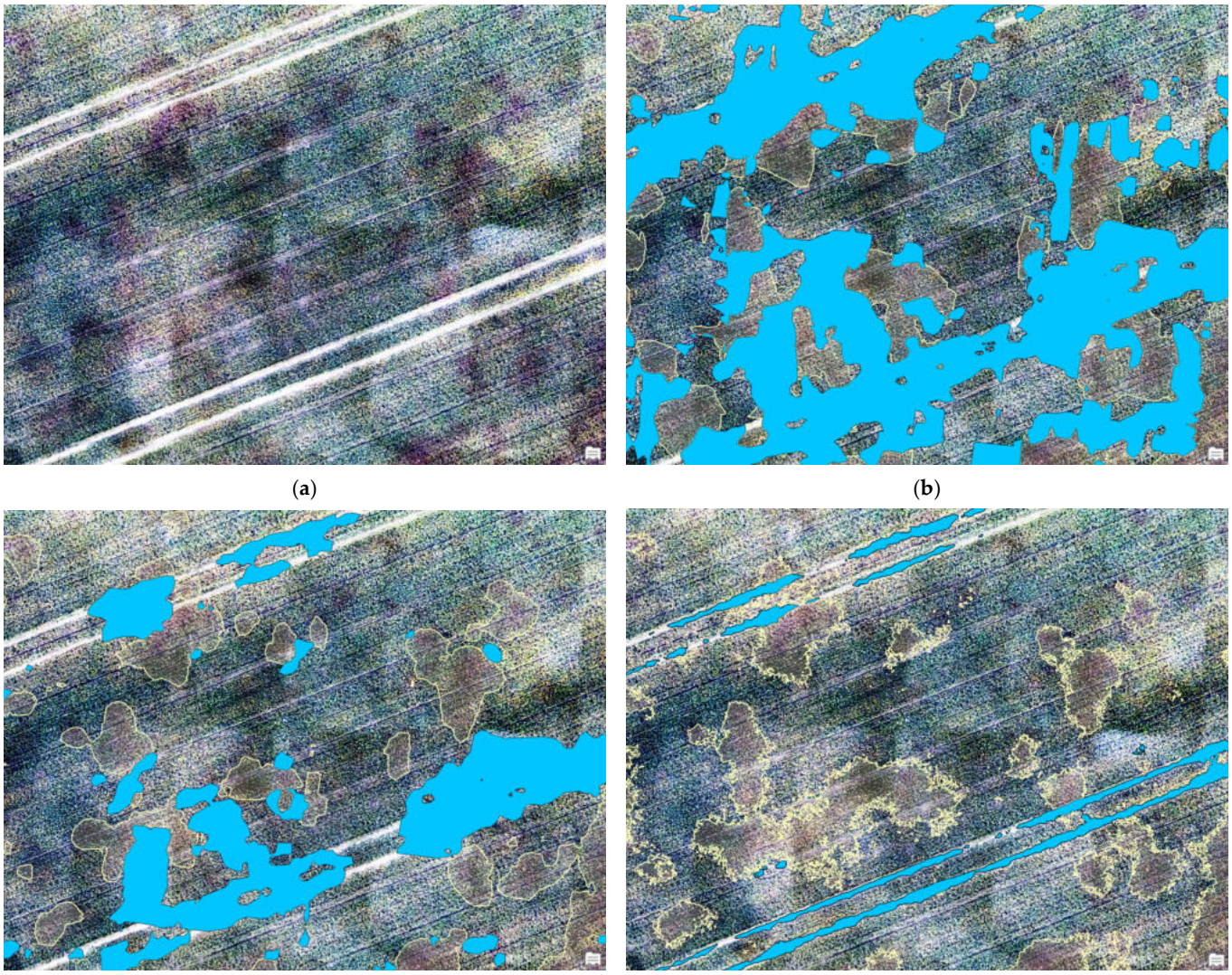

Figure 18. Close-up from the orthomosaic with an equalization filter applied (**a**) and the infested and (surrounded with yellow) and tracks (in blue) areas marked, by the DeepLabv3 + ResNet34 (**b**), DeepLabv3 + ResNet50 (**c**), and U-Net + ResNet101 (**d**) models, respectively.

Different reasons could exist for such misbehavior of the DeepLab-based models. One of them is the quality loss, which occurs when generating the orthomosaic from the original data. It could be speculated that it is caused by the algorithm ArcGIS Pro uses for its compilation. It might be interesting to investigate other orthomosaic generation algorithms; however, this falls outside the scope of the current study. Nevertheless, the obtained results allow us to acknowledge that the DeepLab model is less robust compared to the U-Net model when it comes to the quality of the input data. Furthermore, the obtained results confirm those obtained in [18], that the U-Net architecture performs better, compared to the DeepLab v3 convolutional network, when it comes to identifying different types of diseases in winter wheat.

Even though the U-Net model does not identify all tractor tracks, this is not considered a serious problem, as the main goal of the model is to correctly identify the infested areas. The tractor tracks class was included in the current study only with the idea to limit the false positives when it comes to aphid infestations. The obtained results show that tractor tracks are not misclassified as unhealthy areas with the U-Net-based model, which indicates their inclusion as a class is justified.

The final step of this study is to analyze the obtained orthomosaic with the optimal model in order to assess the infestation of the field. According to the U-Net + ResNet101 model, the investigated field has 1.87 hectares of infested area, 2.14 hectares of healthy area, and 0.14 hectares of tractor tracks. These spatially explicit and quantitatively reliable results provide a solid basis for informed decision-making, enabling targeted pesticide application, optimization of treatment zones, and reduction of unnecessary chemical inputs while maintaining effective control of *Sitobion avenae* infestations.

Despite occasional misclassification of tractor tracks, the overall validation of the models can be considered successful, as the primary objective of this study was the detection of *Sitobion avenae*-infested plants. Tractor tracks are associated with reduced wheat vegetation due to soil compaction, which may contribute to misclassification in these areas. Nevertheless, this does not compromise the applicability of the models for aphid detection. In particular, the U-Net + ResNet101 model demonstrated high accuracy in identifying infested areas, with minimal false negatives and satisfactory precision and recall, providing reliable detection of *Sitobion avenae* infestation despite the confounding influence of tractor tracks.

3.4. Comparison of the Results with Previous Studies

To get a better understanding of the performance of the trained model, it should be compared to those obtained in previous studies. In ref. [37], several machine learning algorithms (Minimum distance—MD, Maximum likelihood—ML, and Support vector machine—SVM) were used on UAV-obtained RGB data from a winter wheat field to identify non-photosynthetic areas and to assess their health degree. The results showed that the Minimum distance algorithms returned the highest performance, reaching a Kappa coefficient of 0.863 and a precision level of 0.856.

In another study [38], multispectral UAV-obtained data were used for early identification of yellow rust in wheat. Four classification algorithms were used—Random forest (RF), SVM, Multi-layer perception (MLP), and three-dimensional convolutional neural network (3D-CNN). The models showed different success rates in different periods of the infestation, with the 3D-CNN model having the highest F1 score in the second period of the experiment. Another study, dealing with yellow rust, investigated the performance of different deep learning models for its identification [18]. Different combinations of neural networks and backbone models were studied, with the U-Net classifier and ResNet34 backbone showing the best performance, reaching an average F1 score of 0.874 and a Kappa of 0.977.

In ref. [24], the machine learning algorithms Logistic regression (LR), k-Nearest neighbor (KNN), SVM, RF, and Light gradient boosting machine (LGBM) were used to identify aphid infestation in winter wheat. Hyperspectral images were used, with the SVM and RF models showing the best performance, reaching an accuracy and F1 score of 0.94.

From the performed overview (Table 7), it can be seen that neural network-based models commonly perform significantly better at identifying different types of diseases in wheat, whether using RGB or hyperspectral data. Furthermore, the models' performance for early-stage detection is lower, which is expected. The results of this study once again confirm that the "histogram equalization" filter, applied on RGB images, provide better results when identifying wheat infestations, compared to pure hyperspectral imagery. In this study, the F1 score and Cohen's Kappa metrics obtained for the best-performing U-Net + ResNet101 model are either slightly higher or comparable to those obtained in previous studies, which indicates the proposed methodology is well applicable for precise identifications of *Sitobion avenae* infestation in winter wheat.

Table 7. Comparison of the results of different studies.

Study	Objectives	Models	Metrics
Du et al. (2025) [37]	Classify non-photosynthetic areas in a winter wheat field with RGB data.	MD, MLE, SVM (optimal)	Kappa: 0.863 Precision: 0.856
Nguyen et al. (2023) [38]	Early identification of yellow rust in wheat with multispectral imagery.	RF, SVM, MLP, and 3D-CNN (optimal)	F1: 0.63–0.78
Atanasov et al. (2025) [18]	Identification of yellow rust in winter wheat using RGB data.	U-Net classifier with ResNet34 backbone	F1: 0.874 Kappa: 0.977
Skendzic et al. (2025) [24]	Identification of Aphid infestation in winter wheat using hyperspectral data.	LR, KNN, LGBM, SVM (optimal, RF (optimal)	Accuracy: 0.94 F1: 0.94
This study	Identification of *Sitobion avenae* in winter wheat with RGB data.	U-Net classifier with ResNet101 backbone	F1: 0.982 Kappa: 0.966

3.5. Practical Implications and Study Limitations

Based on the results obtained from the spatial analysis, an informed assessment of the phytosanitary status of the crop can be performed, enabling timely and data-driven decision-making in pest management. The identification of clearly localized infestation hotspots creates favorable conditions for the application of precision plant protection practices, where insecticides are applied only in affected zones rather than across the entire field. Such an approach allows a substantial reduction in pesticide use, lower production costs, and minimized negative impacts on beneficial insect populations and the surrounding environment.

When low to moderate infestation levels are detected, increased monitoring at short time intervals is recommended, as aphid populations may expand rapidly under favorable meteorological conditions. In this context, UAV-based monitoring represents an effective tool for tracking the spatial and temporal dynamics of *Sitobion avenae* infestations and for determining the moment when the economic damage threshold is reached.

In cases of severe infestation, such as those observed in parts of the investigated field, timely chemical control becomes necessary. The selection of insecticides should be aligned with the crop growth stage and current recommendations for *Sitobion avenae* management. The generated classification maps can be directly used for the creation of variable-rate application maps, representing an important step toward the integration of the proposed methodology into operational precision agriculture systems.

In the long term, the presented approach supports the implementation of integrated pest management (IPM) strategies, where plant protection decisions are based on spatially explicit and objective data rather than solely on visual inspections or field-average estimations.

Despite the encouraging results of the present study, it should be acknowledged that the use of histogram equalization for effective highlighting of infested areas may introduce spectral distortions that affect model performance when applied to large-scale orthomosaics. Furthermore, the study focused exclusively on RGB imagery; therefore, the potential benefits of combining RGB data with multispectral, thermal, or meteorological information were not explored.

4. Conclusions

This study investigates the possibilities for identifying *Sitobion avenae* infestations in winter wheat using UAV-obtained RGB images and deep learning. A methodology for training deep learning models for the identification of the infested areas is summarized. In the current study, three classes were defined: healthy, infested, and tractor tracks. Furthermore, three neural network architectures (U-Net, DeepLab version 3, and PSPNet) in combination with three backbone models (ResNet34, ResNet50, and ResNet101) were investigated. Another important aspect is that the "histogram equalization" filter was used to highlight the infested areas.

Next, the proposed methodology was applied on UAV-obtained experimental RGB dataset from a winter wheat field near Kalipetrovo, Bulgaria. Out of the dataset, 4 images were selected for training and 4 for validation purposes. The validation of the trained models showed that the DeepLab + ResNet50 has the highest performance, closely followed by DeepLab + ResNet34 and U-Net + ResNet101. However, after these three models were applied to the generated orthomosaic, the created classification maps showed that both DeepLab models failed to properly analyze it. The main reason for this is the enormous number of false negatives in the "tractor tracks" class.

The main conclusion from this study is that the U-Net neural network architecture, in combination with a ResNet101 backbone, has the best performance when it comes to identifying *Sitobion avenae* infestations in winter wheat. It reached an F1 score and Cohen's Kappa of 0.982 and 0.966, respectively. Furthermore, it was once again confirmed that the "histogram equalization" filter highlights the infested areas similarly to NDVI, which allows using significantly cheaper visual spectrum cameras instead of multispectral ones.

Future research should focus on extending the proposed approach toward multi-temporal UAV monitoring, enabling early warning and prediction of aphid outbreaks rather than solely their spatial detection. The integration of RGB-based deep learning results with meteorological data, satellite observations, and decision-support systems could significantly enhance precision pest management under changing climatic conditions. Further studies may also investigate advanced deep learning architectures and the direct generation of variable-rate treatment maps, supporting the transition toward fully digital and data-driven crop protection strategies. Another important goal for future studies is to investigate the robustness of the histogram equalization filter when used on RGB images to focus on infested wheat areas.

Author Contributions: Conceptualization, A.Z.A. and B.I.E.; methodology, A.Z.A. and B.I.E.; software, B.I.E.; validation, B.I.E., A.I.A. and P.D.N.; formal analysis, A.Z.A., B.I.E. and A.I.A.; investigation, A.Z.A. and P.D.N.; resources, A.Z.A. and P.D.N.; data curation, B.I.E.; writing—original draft preparation, A.Z.A. and B.I.E.; writing—review and editing, A.I.A. and A.C.; visualization, B.I.E. and A.Z.A.; supervision, A.Z.A.; project administration, A.Z.A.; funding acquisition, A.Z.A. All authors have read and agreed to the published version of the manuscript.

Funding: This study was financed by the European Union—NextGenerationEU, through the National Recovery and Resilience Plan of the Republic of Bulgaria, project № BG-RRP-2.013-0001.

Institutional Review Board Statement: Not applicable.

Data Availability Statement: The data presented in this study are available upon request from the corresponding author.

Acknowledgments: This research was supported by the National Science Fund under grant agreement № КП-06-Н76/2 2023 project "Integration of satellite derived and ground-based data for soil water balance components and crop cover into models for assessment of agroecological risks and agricultural practices for their mitigation".

Conflicts of Interest: The authors declare no conflicts of interest.

Abbreviations

The following abbreviations are used in this manuscript:

UAV	Unmanned Aerial Vehicle
RGB	Red, Green, Blue
NDVI	Normalized Difference Vegetation Index
NDRE	Normalized Difference Red Edge Index
EVI	Enhanced Vegetation Index
ML	Machine Learning
AI	Artificial Intelligence
VTOL	Vertical Take-off and Landing
GSD	Ground Sample Distance

References

1. Shiferaw, B.; Smale, M.; Braun, H.J.; Duveiller, E.; Reynolds, M.; Muricho, G. Crops that feed the world 10. Past successes and future challenges to the role played by wheat in global food security. *Food Sec.* **2013**, *5*, 291–317. [CrossRef]
2. Ayaz, L.S. Wheat Its Grain and Shape. 2020. Available online: https://www.researchgate.net/publication/343136832 (accessed on 20 December 2025).
3. Ministry of Agriculture and Food. Available online: https://www.mzh.government.bg/media/filer_public/2025/09/16/ra460_publicationcrops2024_en.pdf (accessed on 6 January 2026).
4. Agriculture and Climate. Available online: https://www.epa.gov/agriculture/agriculture-and-climate (accessed on 5 March 2026).
5. Bajwa, A.A.; Farooq, M.; Al-Sadi, A.M.; Nawaz, A.; Jabran, K.; Siddique, K.H. Siddique, Impact of climate change on biology and management of wheat pests. *Crop. Prot.* **2020**, *137*, 105304. [CrossRef]
6. Skendžić, S.; Zovko, M.; Živković, I.P.; Lešić, V.; Lemić, D. The Impact of Climate Change on Agricultural Insect Pests. *Insects* **2021**, *12*, 440. [CrossRef]
7. The Influence of Climate Change on Wheat Production. Available online: https://immap.org/wp-content/uploads/2016/12/Review-Study_Climate-Change-and-its-influence-on-Wheat-Production-in-NES.pdf (accessed on 6 January 2026).
8. Kamran, A.; Asif, M.; Bilal, S.; Ahmad, M.; Hirani, A. Major Insects of wheat: Biology and mitigation strategies. In *Crop Production*; IntechOpen: London, UK, 2013. [CrossRef]
9. Dewar, A.M.; Dean, G.J.; Cannon, R. Assessment of methods for estimating the numbers of aphids (Hemiptera: Aphididae) in cereals. *Bull. Entomol. Res.* **1982**, *72*, 675–685. [CrossRef]
10. Giles, K.L.; Jones, D.B.; Royer, T.A.; Elliott, N.C.; Kindler, S.D. Development of a sampling plan in winter wheat that estimates cereal aphid parasitism levels and predicts population suppression. *J. Econ. Entomol.* **2003**, *96*, 975–982. [CrossRef]
11. Padhiary, M.; Saha, D.; Kumar, R.; Sethi, L.N.; Kumar, A. Enhancing precision agriculture: A comprehensive review of machine learning and AI vision applications in all-terrain vehicle for farm automation. *Smart Agric. Technol.* **2024**, *8*, 100483. [CrossRef]
12. Zhang, X.; Han, L.; Dong, Y.; Shi, Y.; Huang, W.; Han, L.; González-Moreno, P.; Ma, H.; Ye, H.; Sobeih, T. A Deep Learning-Based Approach for Automated Yellow Rust Disease Detection from High-Resolution Hyperspectral UAV Images. *Remote Sens.* **2019**, *11*, 1554. [CrossRef]
13. Guo, A.; Huang, W.; Dong, Y.; Ye, H.; Ma, H.; Liu, B.; Wu, W.; Ren, Y.; Ruan, C.; Geng, Y. Wheat Yellow Rust Detection Using UAV-Based Hyperspectral Technology. *Remote Sens.* **2021**, *13*, 123. [CrossRef]
14. Abdulridha, J.; Min, A.; Rouse, M.N.; Kianian, S.; Isler, V.; Yang, C. Evaluation of Stem Rust Disease in Wheat Fields by Drone Hyperspectral Imaging. *Sensors* **2023**, *23*, 4154. [CrossRef]
15. Su, J.; Liu, C.; Chen, W.H. UAV Multispectral Remote Sensing for Yellow Rust Mapping: Opportunities and Challenges. In *Unmanned Aerial Systems in Precision Agriculture*; Zhang, Z., Liu, H., Yang, C., Ampatzidis, Y., Zhou, J., Jiang, Y., Eds.; Smart Agriculture; Springer: Singapore, 2022; Volume 2. [CrossRef]
16. Atanasov, A.I.; Atanasov, A.Z.; Evstatiev, B.I. Application of NDVI for Early Detection of Yellow Rust (*Puccinia striiformis*). *AgriEngineering* **2025**, *7*, 160. [CrossRef]
17. Heidarian Dehkordi, R.; El Jarroudi, M.; Kouadio, L.; Meersmans, J.; Beyer, M. Monitoring Wheat Leaf Rust and Stripe Rust in Winter Wheat Using High-Resolution UAV-Based Red-Green-Blue Imagery. *Remote Sens.* **2020**, *12*, 3696. [CrossRef]
18. Atanasov, A.Z.; Evstatiev, B.I.; Atanasov, A.I.; Nikolova, P.D. Assessment of Yellow Rust (*Puccinia striiformis*) Infestations in Wheat Using UAV-Based RGB Imaging and Deep Learning. *Appl. Sci.* **2025**, *15*, 8512. [CrossRef]

19. Marston, Z.P.D.; Cira, T.M.; Hodgson, E.W.; Knight, J.F.; Macrae, I.V.; Koch, R.L. Detection of stress induced by soybean aphid (Hemiptera: Aphididae) using multispectral imagery from unmanned aerial vehicles. *J. Econ. Entomol.* **2020**, *113*, 779–786. [CrossRef] [PubMed]
20. Zhu, H.; Lin, C.; Liu, G.; Wang, D.; Qin, S.; Li, A.; Xu, J.-L.; He, Y. Intelligent agriculture: Deep learning in UAV-based remote sensing imagery for crop diseases and pests detection. *Front. Plant Sci.* **2024**, *15*, 1435016. [CrossRef]
21. Shahi, T.B.; Xu, C.-Y.; Neupane, A.; Guo, W. Machine learning methods for precision agriculture with UAV imagery: A review. *Electron. Res. Arch.* **2022**, *30*, 4277–4317. [CrossRef]
22. Guo, H.; Cheng, Y.; Liu, J.; Wang, Z. Low-cost and precise traditional Chinese medicinal tree pest and disease monitoring using UAV RGB image only. *Sci. Rep.* **2024**, *14*, 25562. [CrossRef]
23. Ren, C.; Liu, B.; Liang, Z.; Lin, Z.; Wang, W.; Wei, X.; Li, X.; Zou, X. An Innovative Method of Monitoring Cotton Aphid Infestation Based on Data Fusion and Multi-Source Remote Sensing Using Unmanned Aerial Vehicles. *Drones* **2025**, *9*, 229. [CrossRef]
24. Skendzic, S.; Novak, H.; Zovko, M.; Pajač Živković, I.; Lešić, V.; Maričević, M.; Lemić, D. Hyperspectral Canopy Reflectance and Machine Learning for Threshold-Based Classification of Aphid-Infested Winter Wheat. *Remote Sens.* **2025**, *17*, 929. [CrossRef]
25. Ualiyeva, R.M.; Kaverina, M.M.; Osipova, A.V.; Faurat, A.A.; Zhangazin, S.B.; Iksat, N.N. Hyperspectral Imaging and Machine Learning for Automated Pest Identification in Cereal Crops. *Biology* **2025**, *14*, 1715. [CrossRef]
26. Skendžić, S.; Novak, H.; Zovko, M.; Pajač Živković, I.; Lešić, V.; Maričević, M.; Lemić, D. Hyperspectral Sensing and Machine Learning for Early Detection of Cereal Leaf Beetle Damage in Wheat: Insights for Precision Pest Management. *Agriculture* **2025**, *15*, 2482. [CrossRef]
27. Panopoulou, C.; Antonopoulos, A.; Arapostathi, E.; Stamouli, M.; Katsileros, A.; Tsagkarakis, A. Using Multispectral Data from UAS in Machine Learning to Detect Infestation by *Xylotrechus chinensis* (Chevrolat) (Coleoptera: Cerambycidae) in Mulberries. *Agronomy* **2024**, *14*, 2061. [CrossRef]
28. Zhang, S.; Wang, X.; Lin, H.; Dong, Y.; Qiang, Z. A review of the application of UAV multispectral remote sensing technology in precision agriculture. *Smart Agric. Technol.* **2025**, *12*, 101406. [CrossRef]
29. Amarasingam, H.; Powell, K.; Sandino, J.; Bratanov, D.; Salgadoe, A.S.A.; Gonzalez, F. Mapping of insect pest infestation for precision agriculture: A UAV-based multispectral imaging and deep learning techniques. *Int. J. Appl. Earth Obs. Geoinf.* **2025**, *137*, 104413. [CrossRef]
30. Fuentes, S.; Tongson, E.; Unnithan, R.R.; Gonzalez Viejo, C. Early Detection of Aphid Infestation and Insect-Plant Interaction Assessment in Wheat Using a Low-Cost Electronic Nose (E-Nose), Near-Infrared Spectroscopy and Machine Learning Modeling. *Sensors* **2021**, *21*, 5948. [CrossRef] [PubMed]
31. Arshad, I.; Rasul, A.; Hussain, S.; Aslam, H.; Hayat, K.; Hassan, M.; Muqeet, S.; Amina; Umar, Y.; Nasir, S.; et al. Impact of Climate Change on Epidemiology of Various Pests of Wheat Crop in Punjab Pakistan. *Am. J. Plant Sci.* **2019**, *10*, 236–247. [CrossRef]
32. Trifonov, S. Melioration Survey of Hydro-Meliorative Sites. Soil characteristics of lands at Kalipetrovo village, Silistra distrct. In *Soil Archive of ISSAPP "N. Poushkarov"*; Vodproetk: Sofia, Bulgaria, 1986.
33. P4 Multispectral. Available online: https://www.dji.com/bg/p4-multispectral (accessed on 8 January 2026).
34. Liu, Z.; Su, B.; Lv, F. Intelligent Identification Method of Crop Species Using Improved U-Net Network in UAV Remote Sensing Image. *Sci. Program.* **2022**, *2022*, 9717843. [CrossRef]
35. Su, J.; Yi, D.; Su, B.; Mi, Z.; Liu, C.; Hu, X.; Xu, X.; Guo, L.; Chen, W.-H. Aerial visual perception in smart farming: Field study of wheat yellow rust monitoring. *IEEE Trans. Ind. Inform.* **2020**, *17*, 2242–2249. [CrossRef]
36. Deng, J.; Zhou, H.; Lv, X.; Yang, L.; Shang, J.; Sun, Q.; Zheng, X.; Zhou, C.; Zhao, B.; Wu, J.; et al. Applying convolutional neural networks for detecting wheat stripe rust transmission centers under complex field conditions using RGB-based high spatial resolution images from UAVs. *Comput. Electron. Agric.* **2022**, *200*, 107211. [CrossRef]
37. Du, M.; Xie, Z.; Wang, H.; Ji, J.; Jin, X.; Roshanianfard, A. Assessing the health degree of winter wheat under field conditions for precision plant protection by using UAV imagery. *Int. J. Agric. Biol. Eng.* **2025**, *18*, 195–203. [CrossRef]
38. Nguyen, C.; Sagan, V.; Skobalski, J.; Severo, J.I. Early Detection of Wheat Yellow Rust Disease and Its Impact on Terminal Yield with Multi-Spectral UAV-Imagery. *Remote Sens.* **2023**, *15*, 3301. [CrossRef]